MATERIALS CHEMISTRY
FRONTIERS

RESEARCH ARTICLE

View Article Online
View Journal | View Issue

Cite this: *Mater. Chem. Front.*, 2019, **3**, 1786

Zinc porphyrin–polydopamine core–shell nanostructures for enhanced photodynamic/photothermal cancer therapy†

Changjin Ou, ‡[a] Yewei Zhang,‡[b] Dong Pan,[c] Kaikai Ding,[a] Shichao Zhang,[a] Wenjing Xu,[b] Wenjun Wang,[d] Weili Si, *[a] Zhou Yang *[c] and Xiaochen Dong *[a]

Received 30th March 2019,
Accepted 21st June 2019

DOI: 10.1039/c9qm00197b

rsc.li/frontiers-materials

Multimodal therapy, integrating two or more compositions with different functions into a nanoplatform, will generate the synergistic effects of the multi-components and effectively improve the tumor therapeutic efficacy. Herein, core–shell structured ZnP@PDA nanoparticles (NPs) were easily constructed *via* encapsulating the near-infrared (NIR) photosensitizer of zinc porphyrin nanoparticles (ZnP NPs) with polydopamine (PDA). The ZnP@PDA NPs displayed good biocompatibility and could effectively prevent aggregation after intravenous injection. Triggered by a NIR laser, the ZnP@PDA NPs exhibited excellent photodynamic performance. Furthermore, compared with PDA or ZnP NPs, the ZnP@PDA NPs showed improved photothermal performance with a high photothermal conversion efficiency (PCE) of 46.8% due to the triplet exciton quenching and fluorescence resonance energy transfer (FRET). *In vitro* and *in vivo* evaluations demonstrated that the ZnP@PDA NPs could directly target the tumor site *via* the enhanced permeability and retention (EPR) effect and exhibited strong phototoxicity and outstanding tumor phototherapeutic efficacy.

Introduction

Photothermal therapy (PTT) has been recognized as a promising approach for cancer treatment due to its minimal invasion, low side effects and high specificity.[1] The photothermal agent (PTA) of PTT can convert the absorbed light energy to heat which results in localized hyperthermia and induces the ablation of tumor cells. Many efforts have been made to explore novel PTAs with high light-absorbing ability and photothermal conversion efficiency (PCE).[1] The PCE of organic dye nanoparticles could be finely tuned and was up to around 60% *via* molecular engineering.[2–4] However, the temperature elevation is inhomogeneous in tumor tissue during irradiation since light intensity decreases quickly with the increase in penetration depth. The cell damage caused by heating in the deep region may be repaired with the help of heat-shock proteins, which would enhance the heat resistance and reduce the therapeutic efficacy of PTT.[5,6] To overcome this issue, one of the promising solutions is developing multimodal therapy, for example, the combination of PTT with photodynamic therapy (PDT) or chemotherapy.[7–14] The tumor cells where the PTT doesn't work can be eliminated by the cytotoxic reactive oxygen species (ROS), mainly singlet oxygen ($^1O_2$), achieving an enhanced tumor phototherapeutic efficacy. However, PDT and PTT exhibit mutual competition, and efficient construction of multifunctional nanocomposites is still a challenge.

The core and shell can serve different functions so that the core–shell nanostructure can provide an opportunity to precisely control the physical, chemical and biological properties of the nanoparticles.[15–17] It has been reported that photosensitizers as the core surrounded by amorphous SiO_2 could present higher $^1O_2$ generation yield.[18,19] However, the SiO_2 shell did not have a photothermal effect, and the nano-composite only enabled mono-modal therapy. To realize multimodal tumor phototherapy, generally, a PTA as the core was loaded with photosensitizers (PSs) or chemotherapeutic drugs by covalent binding or absorption. And photothermal nanomaterials, such as gold nanorods, black phosphorus, CuS, polydopamine (PDA), WS_2, and organic semiconductor dots, were frequently married with ICG, chlorin e6 (Ce6), and porphyrin derivatives to fabricate multimodal phototherapeutic agents.[8,15,20–28] While these nanocomposites require

[a] *School of Physical and Mathematical Sciences, Key Laboratory of Flexible Electronics (KLOFE) & Institute of Advanced Materials (IAM), Nanjing Tech University (NanjingTech), Nanjing 211800, China. E-mail: iamxcdong@njtech.edu.cn, iamwlsi@njtech.edu.cn*
[b] *Department of Hepatobiliary and Pancreatic Surgery, Zhongda Hospital, Medical School, Southeast University, Nanjing 210009, China*
[c] *School of Materials Science and Engineering, University of Science and Technology Beijing, Beijing, China. E-mail: yangz@ustb.edu.cn*
[d] *School of Physical Science and Information Technology, Liaocheng University, Liaocheng 252059, China*

† Electronic supplementary information (ESI) available. See DOI: 10.1039/c9qm00197b

‡ These authors contributed equally.

complicated fabrication processes, it is highly desired to develop multimodal nano-medicines only containing the core and shell, which can serve as PTAs and PSs, respectively.

Because of its well-adhesive property, PDA has been widely used as a polymer coating material and functionalized a series of substrates with different surface performances ranging from hydrophile to superhydrophobe.[29] More importantly, PDA displays high PCE, good biocompatibility, no cytotoxicity, and easy functionalization, which makes it an excellent PTA for *in vivo* tumor treatment.[30] For example, Lu *et al.* reported that NIR absorbing PDA-melanin colloidal nanospheres for photothermal therapy had a high PCE of 40% and excellent biocompatibility.[31] Therefore, it is possible and necessary to fabricate PDA based core–shell nano-composites for enhanced PDT/PTT synergistic cancer therapy.

Herein, core–shell structured ZnP@PDA nanospheres were easily constructed through encapsulating the photosensitizer ZnP by PDA. Due to the overlap between the emission of the ZnP NPs and the absorption of PDA, the fluorescence of ZnP is dramatically quenched by the PDA shell *via* fluorescence resonance energy transfer (FRET), which would improve the photothermal performance of PDA to achieve high photothermal conversion efficiency. The excellent biocompatibility of PDA also decreases the dark toxicity of the PDA-functionalized ZnP NPs. Furthermore, ZnP@PDA not only exhibited an outstanding photodynamic effect but also presented an enhanced PCE of 46.8%. *In vitro* and *in vivo* experiments demonstrated that the ZnP@PDA possessed strong phototoxicity to cancer cells.

Experimental section

Chemicals and characterization

2′,7′-Dichlorofluorescein diacetate (DCFH-DA), singlet oxygen sensor green (SOSG) and 4′,6-diamidino-2-phenylindole (DAPI) were purchased from Sigma-Aldrich (MO, USA). Dopamine hydrochloride, tris base and other raw materials were purchased from Adamas reagent (China) and used without further purification. Absorption spectra were measured with a Shimadzu UV-3600 UV-Vis-NIR spectrophotometer. Fluorescence spectra were measured with a Hitachi F-7000 spectrometer. All experiments were conducted in compliance with relevant laws and agency guidelines, and the institutional committee has approved the experiments.

Preparation of ZnP@PDA

ZnP was synthesized according to the literature.[32] A solution of ZnP in tetrahydrofuran (2 mg mL^{-1}, 1 mL) was slowly added into deionized water (10 mL) under vigorous stirring in ambient atmosphere. After 10 minutes, the solution was stirred at 45 °C overnight to remove the tetrahydrofuran. Finally, a green and transparent aqueous solution was obtained with a concentration of 200 μg mL^{-1}.

Tris base (11 mg) and dopamine hydrochloride (5 mg) were dissolved in deionized water and sonicated for two minutes to form a uniform solution. The ZnP nanoparticle solution (200 μg mL^{-1}, 1 mL) was added into the as-prepared solution drop by drop and vigorously stirred at room temperature for 4 hours. The colour of the solution changed from green to dark green. The solution was centrifuged and washed with deionized water three times, and then was further freeze-dried to obtain the ZnP@PDA NP powder.

Singlet oxygen detection

The singlet oxygen sensor green (SOSG) reagent was used to determine the $^1O_2$ generation in the ZnP NPs and ZnP@PDA NPs aqueous solution. Briefly, the SOSG was dissolved in methanol, and then added into different sample solutions ([SOSG] = 2.5 μM, [ZnP NPs] = 5 μg mL^{-1} and [ZnP@PDA NPs] = 5 μg mL^{-1}); after being excited with a 660 nm laser (24 mW cm^{-2}), the mixed solution was excited (excitation wavelength: 494 nm), and then the fluorescence was measured between 510 and 800 nm. The enhanced fluorescence intensity (532 nm) could qualitatively analyze the production of reactive oxygen species.

MTT assay based on HeLa cells

The DMEM high-glucose medium was used to dilute the concentration of the PDA, ZnP NPs and ZnP@PDA NPs to form a concentration gradient. In brief, the HeLa cells were divided into light group and dark group (96-well plates). After dosing for 24 hours, the dark group was placed in darkness and the light group was irradiated with a 660 nm laser (0.8 W cm^{-2}) for 5 minutes. After that, the HeLa cells in the two 96-well plates were cultured for another 12 h, and then MTT solution (5 mg mL^{-1}, 20 μL) was added to each well of the 96-well plate. The cells were incubated for another 4 hours. All the liquid in the well plate was sucked out by a pipettor and 150 μL of DMSO was added to each well. Finally, absorbance was quantified with a Bio-Tek microplate reader (492 nm).

Cellular uptake and fluorescence images

2 mL of HeLa cells was added into two confocal dishes with incubation for 24 h. The ZnP NP and ZnP@PDA NP solutions were diluted with DMEM high-glucose media to 6.6 μg mL^{-1}, respectively. The original cell cultures in the confocal small dishes were aspirated. The ZnP NP and ZnP@PDA NP cell cultures were added to the two confocal small dishes (2 mL), respectively. After 24 h, the HeLa cells were immobilized with paraformaldehyde, and the nuclei of the HeLa cells were stained with the nuclear-specific dye DAPI. After washing three times, the imaging was observed under an inverted microscope (Olympus IX70), excited at the wavelength of 488 nm.

HeLa cells were incubated with 2 mL of the ZnP NP and ZnP@PDA NP (6.6 μg mL^{-1}) solution in confocal dishes for 24 h at 37 °C in a humidified 5% CO_2 atmosphere, respectively. The HeLa cells were immobilized with paraformaldehyde. Then the nuclei of the HeLa cells were stained with the nuclear-specific dye DAPI, and the cells were further incubated with 2′,7′-dichlorofluorescein diacetate (DCFH-DA, 10 μM) for another 30 minutes. After irradiation under a laser (0.8 W cm^{-2}) for 5 minutes, the cellular ROS fluorescence images were observed by an inverted microscope (Olympus IX 70), and excited at the wavelength of 488 nm.

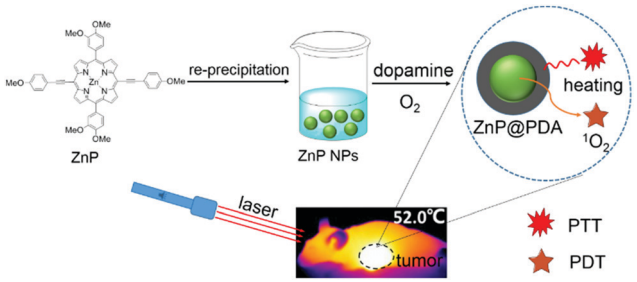

Scheme 1 Schematic illustration for the synthesis of the ZnP@PDA NPs and their application in cancer phototherapy under laser irradiation.

In vivo photothermal and fluorescence imaging

Fluorescence imaging. ZnP@PDA NPs in PBS solution (40 μg mL^{-1}, 100 μL) were injected into HeLa tumor-bearing mice *via* the tail vein. Fluorescence imaging of the tumors was recorded at different times (0, 2, 4, 6, 8, 10, 12, 24, 48 and 72 h) by a fluorescence imaging system (Bruker *In Vivo* Imaging System Fx Pro.). After injection for 24 h, one of the mice was sacrificed, and the tumors and main organs were obtained and imaged immediately to investigate the drug tissue distribution.

Photothermal imaging. ZnP@PDA NPs in PBS solution (40 μg mL^{-1}, 100 μL) or 100 μL PBS solution were injected into HeLa tumor-bearing mice *via* the tail vein, respectively. Photothermal imaging of tumors was monitored at different times irradiated by a laser (660 nm, 0.75 W cm^{-2}) after 6 h injection.

In vivo tumor treatment and histology examination

Fifteen purchased nude mice were injected with HeLa cells into the armpit as the tumor source. When the tumor volumes reached about 100 mm^3, these tumor-bearing nude mice were randomly divided into three groups. Groups 2 and 3 were tail-vein injected with the ZnP@PDA NPs in PBS solution (40 μg mL^{-1}, 100 μL), respectively. Group 1 was injected with normal saline in the same way as the control one. After 6 h, the nude mice of the groups 1 and 3 were irradiated by a laser (660 nm, 0.75 W cm^{-2}) for 5 minutes. The tumor size/body weight of the mice was recorded every two days. The mice were injected with medicine and treated every two days in the same way, and treated for 16 days. After treatment for 16 days and observation for another 14 days, the mice were sacrificed and the histology analysis was carried out. The heart, liver, spleen, lungs, kidneys and tumors were dissected and stored in 4% formaldehyde solution. After dehydration, the tissues were embedded in paraffin boxes and stained with hematoxylin and eosin (H&E). The images were recorded on a PerkinElmer IVIS Lumina K (Scheme 1).

Results and discussion

Preparation and characterization of the nanoparticles

To obtain core–shell nanostructure, firstly, ZnP nanoparticles (ZnP NPs) were prepared *via* re-precipitation methods. Then, the self-polymerization-formed PDA with good adhesive property was easily coated onto the surface of the ZnP NPs to form

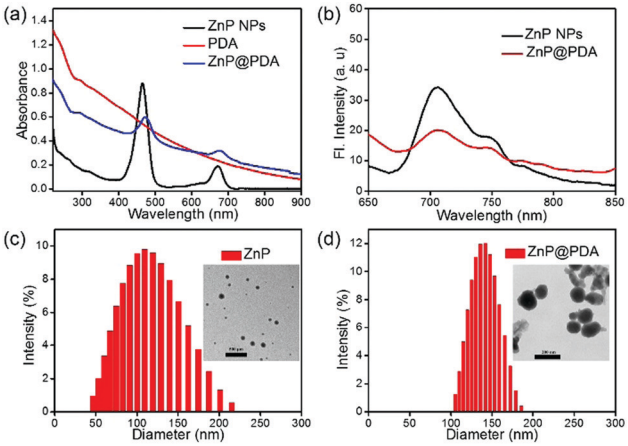

Fig. 1 (a) Absorption spectra of the ZnP NPs, PDA and ZnP@PDA NPs in aqueous solution. (b) Emission spectra of the ZnP NPs and ZnP@PDA NPs in aqueous solution. (c) DLS size distribution of the ZnP NPs. Inset: TEM image of the ZnP NPs, scale bar: 500 nm. (d) The DLS size distribution of the ZnP@PDA NPs. Inset: TEM image of ZnP@PDA NPs, scale bar: 200 nm.

ZnP@PDA NPs. As shown in Fig. 1a, the absorption spectrum of PDA extends to the near infrared region, and the ZnP NPs have two absorption peaks at 464 and 673 nm, respectively. And, the absorption spectrum of the ZnP@PDA NPs contains the characteristic absorption peaks of the ZnP NPs and PDA. Due to the overlap between the emission of the ZnP NPs and the absorption of PDA, the fluorescence of ZnP is dramatically quenched by the PDA shell *via* fluorescence resonance energy transfer (FRET), which results in low emission intensity of the ZnP@PDA NPs (Fig. 1b). The morphologies and sizes of the ZnP NPs and ZnP@PDA NPs were characterized by transmission electron microscopy (TEM) and dynamic light scattering (DLS). As depicted in the inset of Fig. 1c and d, both the ZnP NPs and ZnP@PDA NPs have spherical nanostructures, and the core–shell structure of the ZnP@PDA NPs can be observed clearly. Furthermore, the average hydrodynamic diameters increase from 110 ± 53 nm of the ZnP NPs to 140 ± 35 nm of the ZnP@PDA NPs. These results demonstrated that PDA was successfully coated onto the surface of the ZnP NPs and core–shell structured ZnP@PDA NPs were formed. As shown in Fig. S1 (ESI†), the size distribution of the ZnP@PDA NPs does not show much change after one-week of storage at room temperature, indicating that it is stable in physiological conditions. In addition, the diameter of the NPs was mostly below 200 nm, which can be utilized for passive targeting of the tumor through the EPR effect.[33]

Photodynamic properties

Using singlet oxygen sensor green (SOSG) as a probe, the $^1O_2$ generation ability of the ZnP NPs and ZnP@PDA NPs in aqueous solution was explored. Since strong Q band absorption of the ZnP core can be observed at around 674 nm, a 660 nm laser was used as an excitation source. As shown in Fig. 2a, the fluorescence intensity of SOSG does not show any obvious change during the experimental time, indicating that SOSG is photostable. After incubating with the ZnP NPs and ZnP@PDA

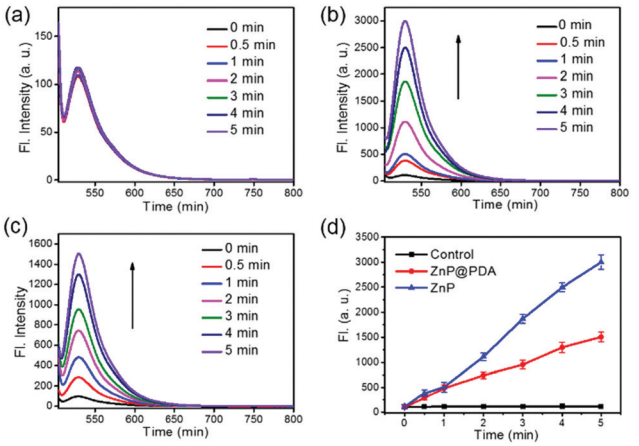

Fig. 2 Fluorescence enhancement of SOSG as a function of laser irradiation time (660 nm, 24 mW cm^{-2}) of (a) SOSG, (b) ZnP NPs, and (c) ZnP@PDA NPs. (d) The fluorescence intensity of SOSG, ZnP NPs and ZnP@PDA NPs at the peak of 532 nm for different irradiation times. The concentrations of the ZnP NPs and ZnP@PDA NPs were 5 μg mL^{-1}.

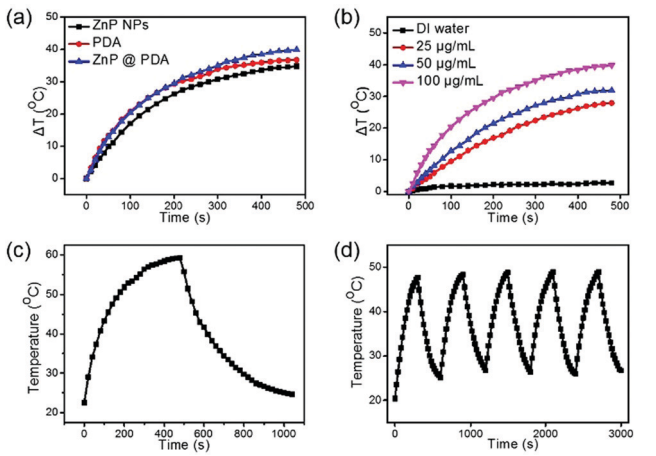

Fig. 3 (a) The photothermal effects of the ZnP NPs, PDA and ZnP@PDA NPs at the same concentrations (100 μg mL^{-1}, 0.8 W cm^{-2}). (b) The photothermal effect of different concentrations of the ZnP@PDA NPs under laser power irradiation of 0.8 W cm^{-2}. (c) The photothermal effect of the aqueous ZnP@PDA NPs (100 μg mL^{-1}, 0.80 W cm^{-2}). The laser was turned off after irradiation for 8 minutes. (d) Photothermal stability of the ZnP@PDA for five alternate on/off laser irradiation cycles (50 μg mL^{-1}, 0.8 W cm^{-2}). All the above experiments were irradiated under a 660 nm laser.

NPs at the same concentrations, respectively, the fluorescence of the SOSG at 532 nm increases rapidly in both samples. The increase of fluorescence intensity is proportional to the irradiation time, while the $^1O_2$ generation rate of the ZnP@PDA NPs drops to about half of that of the ZnP NPs (Fig. 2b–d). It has been reported that the PDA did not show $^1O_2$ generation ability;[30] $^1O_2$ generation was totally contributed by the ZnP NP core. This implies that the PDA shell does not dramatically quench triplet excitons generated by the ZnP core due to the long diffusion length of the triplet excitons,[34] and the ZnP@PDA NPs still exhibit good $^1O_2$ generation ability.

Photothermal properties

The photothermal properties of PDA, ZnP NPs and ZnP@PDA NPs were further evaluated. As shown in Fig. 3a, at the same concentration (100 μg mL^{-1}) and irradiation power (0.8 W cm^{-2}), the temperature change (ΔT) after 6 minutes is 34.8, 36.7 and 39.9 °C for ZnP NPs, PDA and ZnP@PDA NPs, respectively, suggesting that ZnP@PDA displays the best photothermal performance. As illustrated in Fig. 3b and Fig. S3 (ESI†), the ΔT of the ZnP@PDA NPs is positively correlated with the concentration and power density, indicating that the concentration of the ZnP@PDA NPs has a great influence on photothermal therapy. When the concentration of ZnP@PDA NPs reaches 100 μg mL^{-1}, the ΔT of the solution rapidly increases about 20 °C in 100 seconds, which strongly proves the excellent photothermal performance of the ZnP@PDA NPs. Moreover, the PCE of the ZnP@PDA NPs was calculated to be 46.8% based on the data of Fig. 3c and Fig. S4 (ESI†), which was higher than that of the ZnP NPs (33.4%) and PDA (40%),[31,35] and comparable with those of the previously reported PTAs (Table S1, ESI†). The high PCE of the ZnP@PDA NPs mainly originates from FRET and partial triplet exciton quenching. In addition, the ZnP@PDA NPs also display good photothermal stability under continuous laser on/off irradiation for 50 minutes (Fig. 3d), indicating that the ZnP@PDA NPs can be further employed for tumor phototherapy.

In vitro cytotoxicity

A 3-(4,5-Dimethylthiazol-2)-2,5-diphenyltetrazolium bromide (MTT) assay based on HeLa cells was performed to evaluate the biocompatibility and phototoxicity of the ZnP NPs, PDA and ZnP@PDA NPs. As shown in Fig. 4, without the irradiation of a 660 nm laser, the cell viability was still over 91% cultured with PDA and ZnP@PDA NPs at the concentration of 12 μg mL^{-1}, while the cell viability cultured with ZnP NPs was 84%. This indicates that PDA has excellent biocompatibility, and the PDA-functionalized ZnP NPs can reduce dark toxicity and improve biocompatibility. On the contrary, the cell viability was dramatically

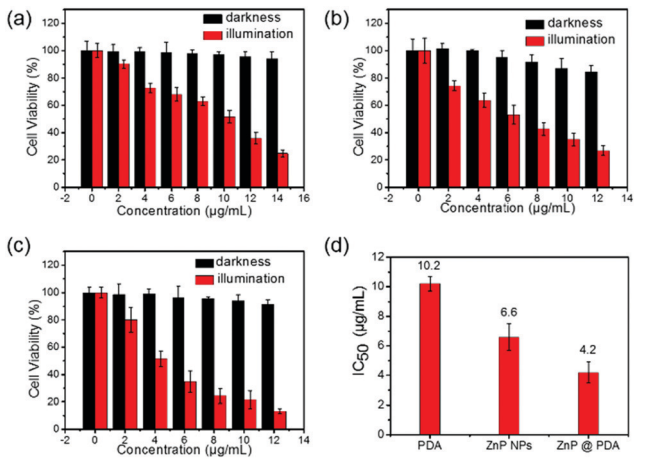

Fig. 4 Cell viability of HeLa cells cultured with different concentrations of (a) PDA, (b) ZnP NPs, and (c) ZnP@PDA NPs with and without laser irradiation. (d) The IC_{50} value of PDA, ZnP NPs and ZnP@PDA NPs.

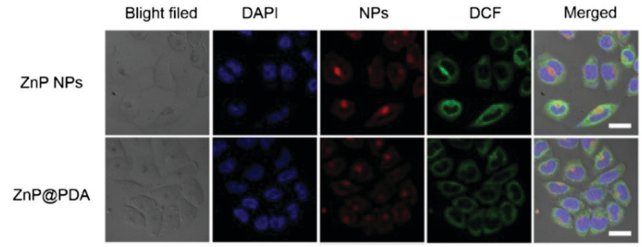

Fig. 5 Cellular uptake of ZnP NPs and ZnP@PDA NPs in HeLa cells with a concentration of 6.6 μg mL^{-1} and the ROS with DCFH-DA as a probe (scale bar: 20 μm).

decreased with the increase in nanoparticle concentration under 660 nm laser irradiation. The half maximal inhibitory concentrations (IC_{50}) of PDA, ZnP NPs, and ZnP@PDA NPs were 10.2, 6.6 and 4.2 μg mL^{-1}, respectively, confirming the enhanced photodynamic/photothermal effects of the core–shell structured ZnP@PDA NPs.

Since both the ZnP NPs and ZnP@PDA NPs show weak fluorescent emission around 705 nm, the cellular uptake can be visualized *via* confocal microscopy. As demonstrated in Fig. 5, the red fluorescence locating in the cytoplasm indicates that the ZnP NPs and ZnP@PDA NPs can be effectively internalized and dispersed in the cytoplasm of HeLa cells. In addition, 2′,7′-dichlorofluorescein diacetate (DCFH-DA) was used as an intracellular ROS probe to monitor the ROS production of the ZnP@PDA NPs *in vitro* (HeLa cells). The HeLa cells were incubated with ZnP@PDA NPs for 24 h, and then irradiated with a 660 nm laser for 5 minutes. As shown in Fig. 5, the bright green fluorescence can be observed clearly in the cytoplasm, indicating that the ZnP@PDA NPs could generate ROS efficiently in HeLa cells. Compared with ZnP NPs, the intensity of green fluorescence was slightly weaker than that with the ZnP@PDA NPs, suggesting that the production of ROS was slightly decreased. This was consistent with the result of the SOSG probe detection. In contrast, no green fluorescence was observed in the PBS solution or PDA NPs (Fig. S5, ESI†). Taken all together, it can be concluded that the core–shell structured ZnP@PDA NPs improve the biocompatibility, decrease low dark toxicity, and enhance phototoxicity. So, the ZnP@PDA NPs can be used as a photothermal/photodynamic synergistic agent for tumor treatment.

In vivo imaging and tumor therapy

To verify the feasibility of the ZnP@PDA NPs for *in vivo* oncotherapy, fluorescence imaging and phototherapeutic studies of ZnP@PDA NPs were performed by using HeLa tumor-bearing mice as models. The ZnP@PDA NPs in PBS solution were intravenously injected into nude mice. Fig. 6a and Fig. S6 (ESI†) show *in vivo* fluorescence imaging and tissue distribution of the ZnP@PDA NPs after drug injection at different times. Six hours after tail intravenous injection, the fluorescence intensity at the tumor site was relatively strong, indicating that the ZnP@PDA NPs have been aggregated into the tumor site through the EPR effect. And 24 hours after injection, the fluorescence signal began to weaken, indicating that the ZnP@PDA NPs decrease *via* metabolizing. A tumor-bearing mouse was executed and dissected after injection for 24 hours,

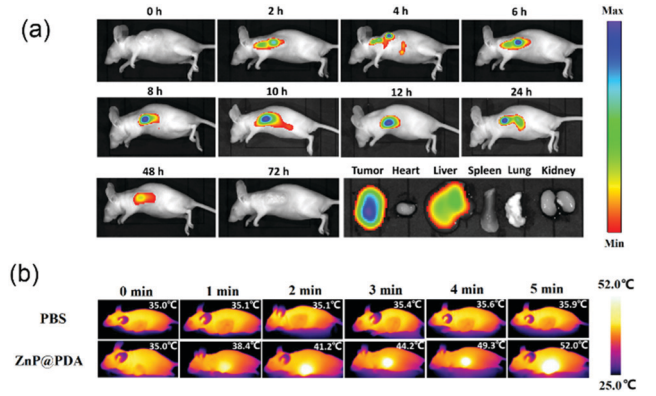

Fig. 6 (a) *In vivo* fluorescence imaging after the injection of ZnP@PDA (40 μg mL^{-1}, 100 μL) and drug tissue distribution after 24 h. (b) *In vivo* photothermal images of the tumor sites after intravenous injection of the ZnP@PDA NPs and PBS.

and its major organs and tumor were taken for fluorescence detection. As shown in Fig. 6a, the fluorescence signal of the ZnP@PDA NPs was mainly located in the tumor, and there was also a relatively strong signal in the liver, denoting that the main metabolic pathway of the drugs was through liver metabolism. After injection for 48 hours, the fluorescence signal of the drug can still be detected, and it still mainly stays in the tumor. However, almost no fluorescence signal was detected in tumor-bearing mice after injection for 48 hours, indicating that the *in vivo* clearance time of the ZnP@PDA NPs was approximately 48 hours. Fig. 6b and Fig. S7 (ESI†) show the photothermal images of the tumor after intravenous injection of ZnP@PDA NPs to mice at different times. After injection of the ZnP@PDA NPs for 6 hours, the temperature of the tumor quickly elevated to 52.0 °C within 5 min, which was high enough to effectively ablate the tumor cells. In contrast, when the PBS-injected mice in the control group were exposed to continuous laser irradiation for 5 min, the temperature only increased about 1 °C, confirming that the laser irradiation did not have an obvious photothermal effect.

During the treatment of nude mice, the changes of tumor volume and mouse body weight were recorded every two days. As shown in Fig. 7a, the average weights of the three groups of mice increased slightly, which directly indicated that the ZnP@PDA NPs had low physical toxicity and good biocompatibility. As shown in Fig. 7b, the tumor volumes in the control and no illumination groups increased dramatically as time went by, while the tumor volume in the illumination group gradually decreased in the first 8 days, and left only a black knot for the next 8 days. After treatment for 4 cycles, the tumors of mice in the illumination group nearly disappeared. These treated mice were kept for 30 days, black scabs fell down and no apparent tumor was observed, indicating the tumor did not relapse. The visual photograph of the tumors and tumor-bearing mice after treatment with different groups is presented in Fig. 7c and Fig. S8 (ESI†). In the illumination group, only a scar was left near the armpits of the mice and the tumor could no longer be seen, which visually proved the therapeutic effect of the ZnP@PDA NPs (Fig. 7d).

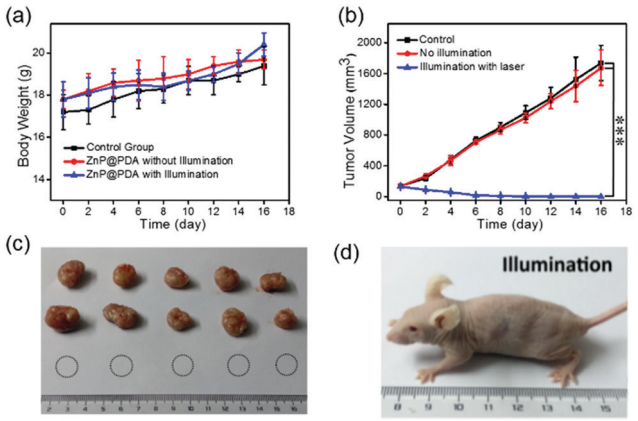

Fig. 7 (a) Body weight changes with time for the control, without illumination and illumination groups. (b) Tumor volume changes with time for the control, without illumination and with illumination groups (n = 5, mean ± SD, ***$p < 0.001$). (c) Different groups of tumors after treatment. (d) Photograph of ZnP@PDA NPs with the illumination group of nude mice after treatment; the tumor almost disappeared.

To further evaluate the therapeutic efficiency, after the treatment, these mice were sacrificed and their major organs (heart, liver, spleen, lung and kidney) and tumors were used for the pathomorphology analysis. As shown in Fig. 8, hematoxylin and eosin (H&E) stained slices showed no significant tissue damage or adverse effects in the major organs of mice after treatment. The excellent therapeutic effect and low dark toxicity of the ZnP@PDA NPs were also observed in Fig. S9 (ESI†). These results further indicated that the ZnP@PDA NPs were essentially non-toxic to normal organs and could effectively inhibit and destroy the tumor cells. Therefore, these experiments *in vivo* manifested that the ZnP@PDA NPs could be used as an efficient therapeutic agent for tumor PDT-enhanced photothermal therapy.

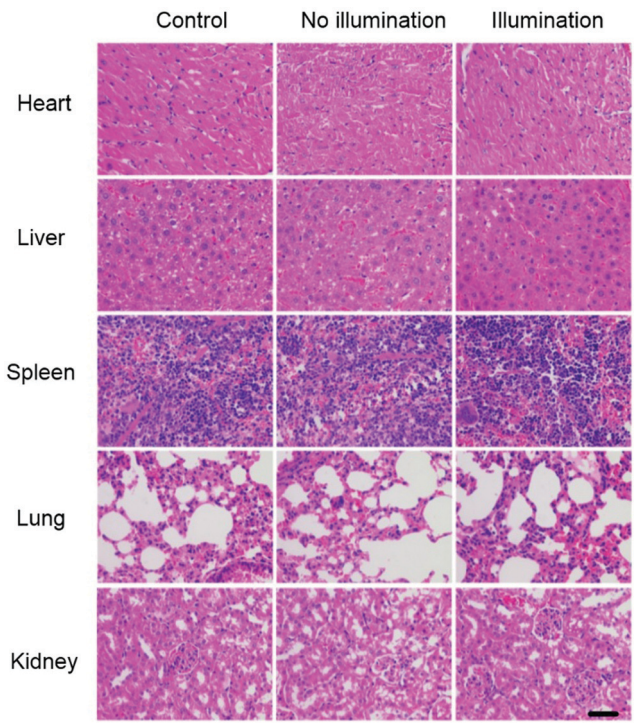

Fig. 8 H&E stained images of the major organs (heart, liver, spleen, lungs, and kidneys) for different groups after treatment (scale bar: 100 μm).

Conclusions

In summary, PDA was successfully encapsulated on the surface of ZnP NPs to construct core–shell structured ZnP@PDA NPs for enhanced photodynamic and photothermal therapy. The ZnP@PDA NPs could enhance the PCE to 46.8% due to exciton quenching and FRET. What's more, although they have PDA coated onto the surface of the ZnP NPs, the core–shell structured ZnP@PDA NPs still keep excellent photodynamic effects. MTT assay and cell imaging results demonstrated that the ZnP@PDA NPs show strong phototoxicity and outstanding biocompatibility. *In vivo* studies further indicate that the ZnP@PDA NPs have excellent PDT/PTT synergistic efficacy and could be utilized as a promising phototherapeutic agent for cancer therapy.

Conflicts of interest

There are no conflicts to declare.

Acknowledgements

The work was supported by the NNSFC (61805117, 51673023, 81872255), Project funded by China Postdoctoral Science Foundation, Six talent peak innovation team in Jiangsu Province (TD-SWYY-009, WSW041), Key medical talents fund of Jiangsu Province (2016KJQWZDRC-03), 333 High-level Talents Training Project (BRA2016508), and Jiangsu Provincial Graduated Training Innovation Project (KYCX18_1125).

Notes and references

1 H. S. Jung, P. Verwilst, A. Sharma, J. Shin, J. L. Sessler and J. S. Kim, *Chem. Soc. Rev.*, 2018, **47**, 2280–2297.
2 P. Liang, Q. Tang, Y. Cai, G. Liu, W. Si, J. Shao., W. Huang, Q. Zhang and X. Dong, *Chem. Sci.*, 2017, **8**, 7457–7463.
3 J. Li, J. Rao and K. Yu, *Biomaterials*, 2018, **155**, 217–235.
4 Y. Cai, W. Si, W. Huang, P. Chen, J. Shao and X. Dong, *Small*, 2018, **14**, 1704247.
5 G. Li, N. F. Mivechi and G. Weitzel, *Int. J. Hyperthermia*, 1995, **11**, 459–488.
6 Y. Yang, W. Zhu, Z. Dong, Y. Chao, M. Chen and Z. Liu, *Adv. Mater.*, 2017, **29**, 1703588.
7 B. Jang, J.-Y. Park, C.-H. Tung, I.-H. Kim and Y. Choi, *ACS Nano*, 2011, **5**, 1086–1094.
8 J. Han, W. Park, S.-J. Park and K. Na, *ACS Appl. Mater. Interfaces*, 2016, **8**, 7739–7747.
9 S. Luo, Z. Yang, X. Tan, Y. Wang, Y. Zeng, Y. Wang, C. Li, R. Li and C. Shi, *ACS Appl. Mater. Interfaces*, 2016, **8**, 17176–17186.

10 S. Wang, P. Huang, L. Nie, R. Xing, D. Liu, Z. Wang, J. Lin, S. Chen, G. Niu, G. Lu and X. Chen, *Adv. Mater.*, 2013, **25**, 3055–3061.
11 Y. Cai, P. Liang, Q. Tang, X. Yang, W. Si, W. Huang, Q. Zhang and X. Dong, *ACS Nano*, 2017, **11**, 1054–1063.
12 X. Yang, D. Wang, Y. Shi, J. Zou, Q. Zhao, Q. Zhang, W. Huang, J. Shao, X. Xie and X. Dong, *ACS Appl. Mater. Interfaces*, 2018, **10**, 12431–12440.
13 Q. Tang, W. Xiao, C. Huang, W. Si, J. Shao, W. Huang, P. Chen, Q. Zhang and X. Dong, *Chem. Mater.*, 2017, **29**, 5216–5224.
14 P. Liang, Y. Wang, P. Wang, J. Zou, H. Xu, Y. Zhang, W. Si and X. Dong, *Nanoscale*, 2017, **9**, 18890–18896.
15 B. Khlebtsov, E. Panfilova, V. Khanadeev, O. Bibikova, G. Terentyuk, A. Ivanov, V. Rumyantseva, I. Shilov, A. Ryabova, V. Loshchenov and N. G. Khlebtsov, *ACS Nano*, 2011, **5**, 7077–7089.
16 J. Yang, D. Shen, L. Zhou, W. Li, X. Li, C. Yao, R. Wang, A. M. El-Toni, F. Zhang and D. Zhao, *Chem. Mater.*, 2013, **25**, 3030–3037.
17 M. Chen, S. Tang, Z. Guo, X. Wang, S. Mo, X. Huang, G. Liu and N. Zheng, *Adv. Mater.*, 2014, **26**, 8210–8216.
18 P. Couleaud, V. Morosini, C. Frochot, S. Richeter, L. Raehm and J.-O. Durand, *Nanoscale*, 2010, **2**, 1083–1095.
19 J. Wang, Y. Zhong, X. Wang, W. Yang, F. Bai, B. Zhang, L. Alarid, K. Bian and H. Fan, *Nano Lett.*, 2017, **17**, 6916–6921.
20 B. Jang, J.-Y. Park, C.-H. Tung, I.-H. Kim and Y. Choi, *ACS Nano*, 2011, **5**, 1086–1094.
21 J. Wang, G. Zhu, M. You, E. Song, M. I. Shukoor, K. Zhang, M. B. Altman, Y. Chen, Z. Zhu, C. Z. Huang and W. Tan, *ACS Nano*, 2012, **6**, 5070–5077.
22 D. Zhang, M. Wu, Y. Zeng, L. Wu, Q. Wang, X. Han, X. Liu and J. Liu, *ACS Appl. Mater. Interfaces*, 2015, **7**, 8176–8187.
23 S. Wang, X. Zhao, S. Wang, J. Qian and S. He, *ACS Appl. Mater. Interfaces*, 2016, **8**, 24368–24384.
24 D. Yang, G. Yang, P. Yang, R. Lv, S. Gai, C. Li, F. He and J. Lin, *Adv. Funct. Mater.*, 2017, **27**, 1700371.
25 J. Peng, L. Zhao, X. Zhu, Y. Sun, W. Feng, Y. Gao, L. Wang and F. Li, *Biomaterials*, 2013, **34**, 7905–7912.
26 W.-S. Kuo, Y.-T. Chang, K.-C. Cho, K.-C. Chiu, C.-H. Lien, C.-S. Yeh and S.-J. Chen, *Biomaterials*, 2012, **33**, 3270–3278.
27 H. P. Tham, H. Chen, Y. H. Tan, Q. Qu, S. Sreejith, L. Zhao, S. S. Venkatraman and Y. Zhao, *Chem. Commun.*, 2016, **52**, 8854–8857.
28 B. Poinard, S. Z. Y. Neo, E. L. L. Yeo, H. P. S. Heng, K. G. Neoh and J. C. Y. Kah, *ACS Appl. Mater. Interfaces*, 2018, **10**, 21125–21136.
29 Y. Liu, K. Ai and L. Lu, *Chem. Rev.*, 2014, **114**, 5057–5115.
30 R. Mrówczyński, *ACS Appl. Mater. Interfaces*, 2018, **10**, 7541–7561.
31 Y. Liu, K. Ai, J. Liu, M. Deng, Y. He and L. Lu, *Adv. Mater.*, 2013, **25**, 1353–1359.
32 K. Ding, Y. Zhang, W. Si, X. Zhong, Y. Cai, J. Zou, J. Shao, Z. Yang and X. Dong, *ACS Appl. Mater. Interfaces*, 2018, **10**, 238–247.
33 Y. Dai, C. Xu, X. Sun and X. Chen, *Chem. Soc. Rev.*, 2017, **46**, 3830–3852.
34 O. V. Mikhnenko, R. Ruiter, P. W. Blom and M. Loi, *Phys. Rev. Lett.*, 2012, **108**, 137401.
35 G. Gollavelli and Y.-C. Ling, *Biomaterials*, 2014, **35**, 4499–4507.

